CHEMISTRY
A EUROPEAN JOURNAL

DOI: 10.1002/chem.200600102

# Gas-Phase Enantioselectivity of Chiral Amido[4]resorcinarene Receptors

**Bruno Botta,[a] Fabiana Caporuscio,[a] Ilaria D'Acquarica,[a] Giuliano Delle Monache,[a] Deborah Subissati,[a] Andrea Tafi,*[b] Maurizio Botta,[b] Antonello Filippi,[a] and Maurizio Speranza*[a]**

**Abstract:** Diastereomeric proton-bound $[\mathbf{1}_L HA]^+$ complexes between selected amino acids (A = phenylglycine (Phg), tryptophan (Trp), tyrosine methyl ester (TyrOMe), threonine (Thr), and allothreonine (AThr)) and a chiral amido[4]resorcinarene receptor ($\mathbf{1}_L$) display a significant enantioselectivity when undergoing loss of the amino acid guest A by way of the enantiomers of 2-aminobutanes (B) in the gas phase. The enantioselectivity of the B-to-A displacement is ascribed to a combination of thermodynamic and kinetic factors related to the structure and the stability of the diastereomeric $[\mathbf{1}_L HA]^+$ complexes and of the reaction transition states. The results of the present and previous studies allow classification of the $[\mathbf{1}_L HA]^+$ complexes in three main categories wherein: i) guest A does not present any additional functionalities besides the amino acid one (alanine (Ala), Phg, and phenylalanine (Phe)); ii) guest A presents an additional alcohol function (serine (Ser), Thr, and AThr); and iii) guest A contains several additional functionalities on its aromatic ring (tyrosine (Tyr), TyrOMe, Trp, and 3,4-dihydroxyphenylalanine (DOPA)). Each category exhibits a specific enantioselectivity depending upon the predominant $[\mathbf{1}_L HA]^+$ structures and the orientation of the 2-aminobutane reactant in the relevant adducts observed. The results may contribute to the understanding of the exceptional selectivity and catalytic properties of enzyme mimics towards unsolvated biomolecules.

**Keywords:** enantioselectivity · gas-phase reactions · host–guest systems · mass spectrometry · molecular dynamics

## Introduction

Biomolecules are often chiral and many biochemical processes show preference of one enantiomer over the other. The exceptional selectivity of biochemical systems is ascribed to size- and shape-specific interactions between large "host" molecules and small "guest" species that bind on or within the host. Usually, the interactions are non-covalent, typically involving van der Waals, electrostatic, or hydrogen-bonding attractions hampered by steric repulsions.

Enzymes exhibit amazing enantioselectivities. Their asymmetric structure is often due to complicated supramolecular assemblies of biopolymers and, therefore, not easily amenable to detailed studies. For this reason, insight into their behavior can be gained by investigating tailor-made simplified host–guest models under conditions, that is, the gas phase, mimicking the extensive desolvation of the guest molecule inside the enzyme cavity.

A number of excellent reviews in the area of gas-phase chiral recognition have recently appeared, which confirm the importance and the broad applicability of this growing field.[1–13] Gas-phase chiral recognition experiments are usu-

[a] Prof. B. Botta, Dr. F. Caporuscio, Dr. I. D'Acquarica, Dr. G. Delle Monache, Dr. D. Subissati, Dr. A. Filippi, Prof. M. Speranza
Dipartimento degli Studi di Chimica e Tecnologia delle Sostanze Biologicamente Attive
Università "La Sapienza"
00185 Roma (Italy)
Fax: (+39) 06-4991-3602
E-mail: maurizio.speranza@uniroma1.it

[b] Prof. A. Tafi, Prof. M. Botta
Dipartimento Farmaco Chimico Tecnologico
Università di Siena
53100 Siena (Italy)
Fax: (+39) 0577-234333
E-mail: tafi@unisi.it

Supporting information for this article is available on the WWW under http://www.chemeurj.org/ or from the author: Ion abundances and kinetic plots of the gas-phase reaction between $[\mathbf{1}_L HA]^+$ (A = Phg, TyrOMe, Trp, Thr, and AThr) and B ($B_R$: black; $B_S$: red; $A_D$: open; $A_L$: full). Docking and Molecular Dynamics Simulations: partial atomic charges, MCMM/MOLS docking and MD graphics.

ally carried out by mass spectrometry through the measurement of: i) the relative abundance of noncovalent diastereomeric adducts between a chiral host and the two enantiomers (one isotopically labeled) of a guest;[1,2,14] ii) the relative stability of diastereomeric adducts by equilibrium measurements[3,6,15,16] or by collision-induced dissociation (CID) experiments (Cooks' kinetic method),[17–25] and iii) the rates of ion/molecule reactions between diastereomeric adducts and suitable chiral or achiral reactants.[5,26–35]

Our group has focused on the last two types of experiments. The emphasis was mainly put on the understanding of the fundamental interactions responsible of chiral discrimination by calixarenes, which have been long recognized as potential enzyme mimics.[36–46] In particular, we used an electrospray-ionization Fourier-transform ion cyclotron resonance mass spectrometer (ESI-FT-ICR) to carry out a kinetic study on the base-induced displacement reaction (1), wherein $[MHA]^+$ are proton-bonded diastereomeric complexes between some representative amino acids (A = Ala, Ser, Leu, Pro, picolinic acid (Pip), Phe, Tyr, DOPA) and suitable calixarene hosts (M), that is, the amido[4]resorcinarene $\mathbf{1}_L$ (Figure 1)[31,32] and most of its isomers,[33] and the enantiomers of 2-aminobutane (B).

$$[MHA]^+ + B \rightarrow A + [MHB]^+ \quad (1)$$

The molecular asymmetry of the selected hosts M is due to the four pendants containing the chiral L-valine group which may be spatially oriented to generate chiral cavities of different size and shape.[33] In the mentioned ESI-FT-ICR studies,[31–33] we pointed out that the efficiency of the gas-phase reaction (1) depends on: i) the configuration of both A and B; ii) the size and the shape of the chiral host M; and iii) the basicity of the amino acid guest A and the nature of its functional groups. For instance, the heterochiral $[\mathbf{1}_L HAla_D]^+$ complex is more reactive than the homochiral $[\mathbf{1}_L HAla_L]^+$ one, whereas the reverse is true for $[\mathbf{1}_L HSer_D]^+$ and $[\mathbf{1}_L HSer_L]^+$. These findings have been explained in terms of the effects of the host asymmetric frame on the structure, stability, and rearrangement dynamics of the diastereomeric $[MHA]^+$ complexes and the orientation of the amine reactant B in encounters with them.

With the aim of elucidating the intrinsic factors, which determine the enantioselectivity in noncovalent host/guest systems, we now extended the investigation to other amino acid guests with different structure and functionalities (i.e., Phg, Trp, and tyrosine methyl ester (TyrOMe)) and with a second chiral center (i.e., Thr and allothreonine (AThr)). The relevant kinetic results will be discussed in the light of molecular mechanics (MM) calculations and molecular dynamics (MD) simulations and compared with those obtained in previous related studies.[31,32]

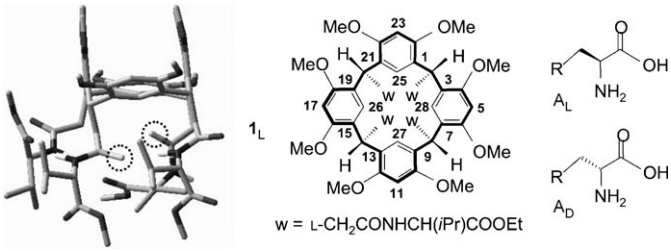


Figure 1. Formula and side view of local minimum geometry of flattened-cone 2,8,14,20-tetrakis(L-valinamido)[4]resorcinarene ($\mathbf{1}_L$).

**Abstract in Italian:** *I complessi diasteromerici non covalenti del tipo $[\mathbf{1}_L HA]^+$, in cui $\mathbf{1}_L$ è un ammido[4]resorcinarene chirale con configurazione definita e A sono gli enantiomeri di alcuni amminoacidi (A = fenilglicina (Phg), triptofano (Trp), tirosina metilestere (TyrMOe), treonina (Thr), and allotreonina (AThr)), mostrano un'elevata enantioselettività quando reagiscono con gli enantiomeri del 2-amminobutano in fase gassosa. L'origine della misurata enantioselettività è attribuita alla combinazione di fattori cinetici e termodinamici ed è principalmente determinata dagli effetti della struttura asimmetrica dell'ammido[4]resorcinarene sulla struttura e la stabilità dei complessi diasteromerici $[\mathbf{1}_L HA]^+$ e delle relative strutture di transizione nel processo di sostituzione dell'amminoacido da parte del 2-amminobutano. Lo studio permette di classificare i complessi $[\mathbf{1}_L HA]^+$ in tre categorie principali dove: i) l'amminoacido non presenta nessun gruppo funzionale ulteriore (alanina (Ala), Phg, and fenilalanina (Phe)); ii) l'amminoacido presenta anche una funzione alcoolica (serina (Ser), Thr, and AThr); e iii) l'amminoacido presenta anche gruppi funzionali nell'anello aromatico (tirosina (Tyr), TyrOMe, Trp, and 3,4-diidrossifenilalanina (DOPA)). Ciascuna categoria mostra una enantioselettività specifica determinata da una struttura predominante per relativo complesso $[\mathbf{1}_L HA]^+$ e dall'orientamento del reagente amminico. I risultati ottenuti contribuiscono allo sviluppo di un modello dinamico per il riconoscimento chirale di biomolecole da parte di enzimi artificiali allo stato non solvatato.*

## Materials and Methods

**Materials**: Enantiomerically pure $\mathbf{1}_L$, in the flattened-cone conformation, was synthesized and purified according to established procedures.[47] The D- and L enantiomers of the amino acids A (A = Phg, Trp, Tyr, Thr, and AThr) were purchased from a commercial source (Aldrich Co.) and used without further purification. The same company provided (*R*)-(−)- ($B_R$) and (*S*)-(+)-2-butylamine ($B_S$), which were purified in the vacuum with several freeze–thaw cycles. A simple and safe procedure was used to prepare the pure enantiomers of TyrOMe: acetyl chloride (5 mL) was added dropwise to cooled dry methanol (50 mL; $T = 0\,^\circ C$), in which the amino acid (1.7 mmol) has been dissolved. The mixture was heated under reflux for about 2 h, and then evaporated to dryness.

**FT-ICR Experiments**: The experiments were carried out as described elsewhere.[31,32] In particular, they were performed at room temperature in an APEX 47e FT-ICR mass spectrometer equipped with an ESI source (Bruker Spectrospin) and a resonance cell ("infinity cell") situated between the poles of a superconducting magnet (4.7 T). Stock solutions of $\mathbf{1}_L$ ($1 \times 10^{-5}$ M) in $H_2O/CH_3OH$ 1:3, containing a fivefold excess of the appropriate amino acid A, were electrosprayed through a heated capillary (130 °C) into the external source of the FT-ICR mass spectrometer.

  

All the formed ions were transferred into the resonance cell by a system of potentials and lenses and quenched by collisions with methane pulsed into the cell through a magnetic valve. Abundant signals, corresponding to the natural isotopomers of the proton-bound complex $[\mathbf{1}_L HA]^+$, were monitored and isolated by broad-band ejection of all the accompanying ionic species. The $[\mathbf{1}_L HA]^+$ family was then allowed to react with the chiral amine B present in the cell at a fixed pressure whose value ranges from $2.3\times10^{-8}$ to $1.3\times10^{-7}$ mbar depending upon its reactivity.

**Computational details**: All computational calculations were carried out on a SGI Origin 300 server and visualized on a SGI Octane workstation. Molecular mechanics (MM) calculations (docking) and molecular dynamics simulations (MD) were performed using the AMBER* force field as implemented in MacroModel 5.5.[48] No cutoff was applied for the non-bonded interactions and the calculations were performed in the gas phase selecting the constant dielectric treatment (dielectric constant $\varepsilon=1.0$). Partial atomic charges to be used in the docking and MD simulations were obtained through quantum-mechanics calculations performed with the semiempirical program MOPAC distributed by Accelrys Inc., using the AM1-Mulliken method. The atomic partial charges used for Trp, Tyr and TyrOMe are reported in the Supporting Information and are specified in the last column of the three Cartesian coordinate structures (.pdb format generated by InsightII) describing the lowest energy conformation of their L enantiomer. The partial charges used for $[\mathbf{1}_L{\cdot}H]^+$ have already been reported elsewhere.[32]

Some insights in the structure and the dynamics of the proton-bound $[\mathbf{1}_L HA]^+$ complexes were obtained by using two computational methodologies, that is, i) the statistical Monte Carlo Multiple Minimum (MCMM) conformational search of A and $[\mathbf{1}_L H]^+$, coupled with random rototranslations of the A guest (MOLS command) relative to the $[\mathbf{1}_L H]^+$ host standing still in the 3D space (MCMM/MOLS docking); and ii) constant temperature MD runs. Although MCMM/MOLS is indeed a well described and validated docking protocol,[32] nevertheless we are aware that the number of rotatable bonds moved in each MCMM/MOLS run (more than 20) is well over the maximum allowed to guarantee exhaustive searches. This problem can be solved by combining docking studies with MD simulations so as to ensure a complete and reasonably homogeneous sampling of the whole potential energy hypersurface of our systems. Each MCMM/MOLS docking run was made of 20000 steps. With A = Tyr and TyrOMe, a total number of 25 torsional degrees of freedom was analyzed, while with A = Trp the number of rotatable bonds was 24. In the docking calculations, the rototranslations of A with respect to $\mathbf{1}_L$ were limited by the maximum values of 180° for the rotational angle and of 3 Å for the translational movement. At the same time, a randomly variable number of rotatable bonds of the side chains of $\mathbf{1}_L$ (the flexibility of the resorcarene skeleton was not directly sampled)[47] and A, ranging from 2 to $N-1$ ($N$ represents the overall number of variable torsion angles defined in the command file), was subjected to random step variations in the range 60–180°. Energy minimizations were performed using the Truncated Newton conjugate gradient (TNCG) procedure and were terminated when the energy gradient root mean square (rms) fell below $10\,J\,mol^{-1}\,Å^{-1}$. To eliminate duplicate conformations, a comparison was performed on the heavy atoms, selecting 1.0 Å as the maximum allowable separation between couples of corresponding atoms after superimposition. All the conformers were saved that differed from the global minimum-energy conformation by less than $20\,kJ\,mol^{-1}$. The overall conformation of each output docking geometry was classified by the values taken by the ad hoc defined structural descriptor (SD) shown in Figure 2a.

The SD shown in Figure 2a with $A = TyrOMe_D$ as guest describes the intermolecular out-of-plane bending defined by picking four atoms as follows: assuming C2 as the carbon bearing the protonated side chain, the four designated atoms were, in sequential order, C28, C25, C27 for the host (Figure 1) and the chiral carbon atom for the guest. The consequence of this choice is that SD values centered around 0° correspond to an external lower rim location of guest A in proximity of the protonated pendant of the host (henceforth denoted as *ext*). Values around −90° suggest a lower rim location of the guest, among the pendants of the hosting resorcin[4]arene (henceforth denoted as *down*), and values of +90° its location into the achiral upper rim cavity (henceforth denoted as *up*). The SD shown in Figure 2b with $A = Tyr_L$ as guest describes the rotation of the $C_{ring}$–$C_\alpha$ bond of the high-energy *up* complex between guest A and a simplified version of $\mathbf{1}_L$.

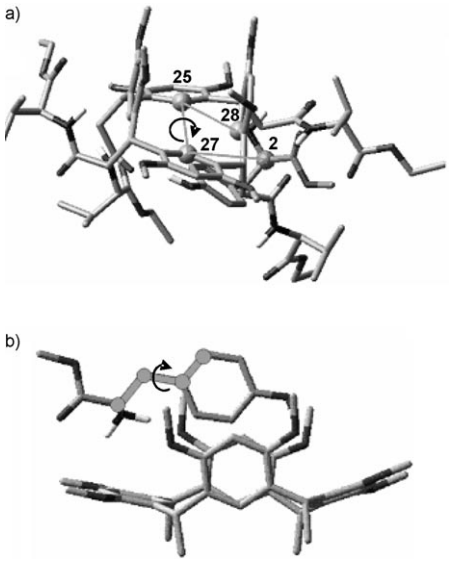


Figure 2. a) Structural descriptor (SD) defined to classify the output MCMM/MOLS docking geometries and to graph MD simulations for $[\mathbf{1}_L HA]^+$; b) Structural descriptor (SD) defined to graph MD simulations for the rotation of the $C_{ring}$–$C_\alpha$ bond of the high-energy *up* complex between A and a simplified version of $\mathbf{1}_L$.

Constant temperature MD simulations with generation of the canonical ensemble were performed at 300 K. Coupling between the temperature bath and the molecules was updated every 0.2 ps. The equilibration period was 50 ps for every run, while the total simulation time was 20 ns. During each trajectory, 5000 structures (frames) were sampled at regular intervals throughout the time course, which were graphed relating SD to the frame number. Each recognition simulation (both docking and molecular dynamics) was repeated few times starting from different arbitrary geometries to produce a complete sampling of the whole potential energy hypersurface of the selected $[\mathbf{1}_L HA]^+$ systems. The convergence of the results guarantees the completeness of the study.

## Results and Discussion

**FT-ICR experiments**: The pseudo-first-order rate constant $k'$ of Reaction (1) was obtained from the slopes of the relevant $\ln(I/I_0)$ versus $t$ plots, where $I$ is the intensity of complex $[\mathbf{1}_L HA]^+$ at the delay time $t$ and $I_0$ is the sum of the intensities of $[\mathbf{1}_L HA]^+$ and $[\mathbf{1}_L HB]^+$ (see, for instance, Figure 3). The corresponding second-order rate constants $k = k'/[B]$ are denoted according to the configuration of the leaving amino acid guest A ($k_D$ or $k_L$) or to that of the amine reactant B ($k_R$ or $k_S$). Enantioselectivity is defined by the $\rho = k_D/k_L$ ratio, when referred to the configuration of the amino acid A, or by the $\xi = k_R/k_S$ one, when referred to the configuration of the amine B. A value of $\rho > 1$ indicates that amine B displaces the D enantiomer of A ($A_D$) faster that the L enantiomer ($A_L$) from the relevant diastereomeric $[\mathbf{1}_L HA_D]^+$ and $[\mathbf{1}_L HA_L]^+$ complexes. The opposite is true when $\rho < 1$. A value $\rho = 1$ corresponds to equal displace-

  

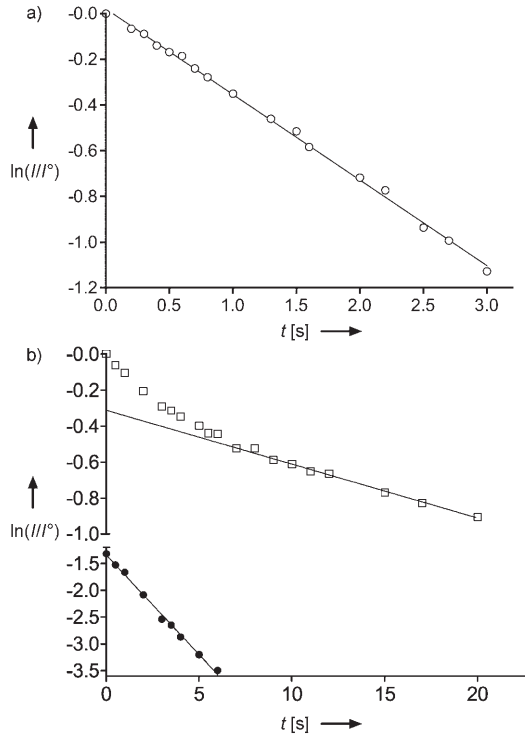


Figure 3. a) Kinetic plot for the gas-phase reaction between (*S*)-(+)-2-butylamine ($p_B = 2.9 \times 10^{-8}$ mbar) and $[\mathbf{1}_L HPhg_D]^+$; b) kinetic plot for the gas-phase reaction between (*R*)-(−)-2-butylamine ($p_B = 1.1 \times 10^{-7}$ mbar) and $[\mathbf{1}_L HTrp_D]^+$.

ment rates. Analogously, a value of $\xi > 1$ indicates that the displacement of the A guest from a given $[\mathbf{1}_L HA]^+$ diastereomer is faster with the (*R*)-amine ($B_R$) than with the (*S*)-one ($B_S$). Again, the opposite is true when $\xi < 1$. A value $\xi = 1$ corresponds to equal displacement rates.

Irrespective of the configuration of B, linear rate plots are observed with A = Phg, Thr, and AThr (corr. coeff. $0.985 < r^2 < 0.998$; see, for instance, Figure 3a), whereas reaction (1) follows bi-exponential kinetics with A = TyrOMe and Trp (see, for instance, Figure 3b). As pointed out in related studies,[5,28,31–33] the bi-exponential kinetics is consistent with the occurrence of two stable isomeric $[MHA]^+$ structures, one less reactive ($[MHA]^+_{slow}$) and the other more reactive ($[MHA]^+_{fast}$). The time dependence of $[MHA]^+_{fast}$ (e.g. solid circles in Figure 3b) can be inferred from the overall $[MHA]^+$ decay (e.g. open squares in Figure 3b) after subtracting the first-order decay of $[MHA]^+_{slow}$ (e.g. upper line in Figure 3b). The two isomeric structures react with the amine B at rates differing by a factor ranging from about 6 to over 16. The *Y* intercepts of the first-order decay of $[MHA]^+_{slow}$ and $[MHA]^+_{fast}$ provide an estimate of their relative distribution. The relevant data are reported in Table 1 together with those concerning the isomeric $[MHA]^+$ (A = DOPA) structures.[33]

The second-order rate constants *k* for all displacement reactions of Equation (1), which have been investigated, are listed in Table 2. Their values, compared with the relevant collision rate constant ($k_{coll}$),[49] provide a measure of the efficiency of the reaction ($eff = k/k_{coll}$). Analysis of Table 2 confirms the view that the efficiency of the gas-phase Reaction (1) depends on the configuration of both A and B and that the corresponding enantioselectivity factors $\rho$ and $\xi$ are dramatically affected by the functional groups present in the amino acid guests. Indeed, those containing an OH functionality, such as Tyr, TyrOMe, DOPA, Ser, Thr, and Athr, confer to the corresponding $[\mathbf{1}_L HA]^+$ complexes a $\rho \leq 1$ factor, while $\rho \geq 1$ factors are invariably measured for the complexes with A = Phg, Phe and Ala. The diastereomeric $[\mathbf{1}_L HA]^+$ (A = Trp) complexes do not follow an univocal trend, since they display $\rho \geq 1$ factors in the reaction with $B_R$ and $\rho < 1$ factors in that with $B_S$. This opposite enantioselectivity is reflected in the corresponding $\xi$ terms which exhibit the largest variation ever measured for this kind of reactions ($\xi = 0.37$–$0.95$). Comparison of the kinetic results of $[\mathbf{1}_L HA]^+$ (A = Tyr, TyrOMe) indicates that the simple methylation of the carboxyl function of the guest induces a dramatic change in the kinetics and the selectivity of Reaction (1). In fact, while $[\mathbf{1}_L HTyr]^+$ follow a mono-exponential decay curve ($\rho \leq 1$; $\xi < 1$), $[\mathbf{1}_L HTyrOMe]^+$ exhibit bi-exponential kinetics ($\rho < 1$; $\xi > 1$) (see Supporting Information and Table 2). Significant enantioselectivity differences have also been noticed for $[\mathbf{1}_L HA]^+$ (A = Ser, Thr, and AThr). Indeed, the complexes with A = AThr appear approximately as selective as those with A = Ser, but appreciably more selective than those with A = Thr, thus indicating that the presence and the configuration of a further chiral center may play a significant role on the reaction (1) efficiency.

Table 1. Percent distribution of isomeric $[\mathbf{1}_L HA]^+$ structures.

| Guest (A) | $[\mathbf{1}_L HA]^+_{fast}$ | $[\mathbf{1}_L HA]^+_{slow}$ |
|---|---|---|
| D-TyrOMe | 20 ± 3 | 80 ± 3 |
| L-TyrOMe | 23 ± 2 | 77 ± 2 |
| D-Trp | 32 ± 5 | 68 ± 5 |
| L-Trp | 35 ± 3 | 65 ± 3 |
| D-DOPA | 20 ± 4 | 80 ± 4 |
| L-DOPA | 19 ± 3 | 81 ± 3 |

The kinetic results of Table 2, in particular the opposite $\rho$ values measured with $[\mathbf{1}_L HTrp]^+$, confirms previous conclusions that the observed enantioselectivities are determined by a combination of kinetic and thermodynamic factors, that is, by the relative stability of the diastereomeric $[\mathbf{1}_L HA]^+$ complexes and by the effects of the resorcin[4]arene frame upon the transition structures involved in their displacement reactions (1). In this view, any attempt of rationalizing the kinetic results of Table 2, in particular the bi-exponential kinetics observed with $[\mathbf{1}_L HA]^+$ (A = TyrOMe, Trp, and DOPA) and the relative enantioselectivities, requires a detailed structural and energetic analysis of the relevant proton-bonded diastereomeric $[\mathbf{1}_L HA]^+$ reactants. This task has been undertaken by using MM calculations and MD simulations.

  

Table 2. Exchange rate constants ($k \times 10^{-10}$ cm$^3$ molecule$^{-1}$ s$^{-1}$).

| Guest (A) | (*R*)-(−)-$C_4H_9NH_2$ | | | (*S*)-(+)-$C_4H_9NH_2$ | | | |
|---|---|---|---|---|---|---|---|
| | $k$ | eff | $\rho$ | $k$ | eff | $\rho$ | $\xi$ |
| D-Phg | 4.98±0.12 | 0.43 | 1.02±0.05 | 5.19±0.06 | 0.45 | 1.22±0.04 | 0.96±0.03 |
| L-Phg | 4.86±0.10 | 0.42 | | 4.24±0.06 | 0.37 | | 1.14±0.05 |
| D-Phe | 3.60±0.03 | 0.32 | 1.64±0.04 | 3.56±0.04 | 0.32 | 1.56±0.04 | 1.01±0.02 |
| L-Phe | 2.20±0.03 | 0.20 | | 2.28±0.04 | 0.21 | | 0.96±0.03 |
| D-Tyr | 0.86±0.02 | 0.08 | 0.80±0.04 | 1.42±0.02 | 0.13 | 1.04±0.03 | 0.61±0.02 |
| L-Tyr | 1.07±0.02 | 0.10 | | 1.36±0.02 | 0.13 | | 0.79±0.02 |
| (D-TyrOMe)$_{fast}$ | 1.63±0.19 | 0.15 | 0.62±0.17 | 1.30±0.04 | 0.12 | 0.72±0.10 | 1.25±0.19 |
| (L-TyrOMe)$_{fast}$ | 2.61±0.30 | 0.23 | | 1.80±0.09 | 0.16 | | 1.45±0.25 |
| (D-TyrOMe)$_{slow}$ | 0.12±0.01 | 0.01 | 0.63±0.06 | 0.08±0.01 | 0.01 | 0.51±0.07 | 1.43±0.15 |
| (L-TyrOMe)$_{slow}$ | 0.18±0.01 | 0.02 | | 0.16±0.01 | 0.01 | | 1.17±0.11 |
| (D-DOPA)$_{fast}$ | 2.28±0.08 | 0.20 | 0.76±0.04 | 1.26±0.05 | 0.11 | 0.69±0.11 | 1.81±0.12 |
| (L-DOPA)$_{fast}$ | 3.00±0.09 | 0.27 | | 1.82±0.20 | 0.16 | | 1.65±0.24 |
| (D-DOPA)$_{slow}$ | 0.07±0.01 | 0.01 | 0.73±0.13 | 0.08±0.01 | 0.01 | 0.81±0.19 | 1.14±0.28 |
| (L-DOPA)$_{slow}$ | 0.10±0.01 | 0.02 | | 0.16±0.01 | 0.01 | | 1.27±0.25 |
| (D-Trp)$_{fast}$ | 1.82±0.04 | 0.16 | 1.60±0.11 | 1.92±0.04 | 0.12 | 0.82±0.10 | 0.95±0.04 |
| (L-Trp)$_{fast}$ | 1.14±0.04 | 0.10 | | 2.33±0.20 | 0.16 | | 0.49±0.06 |
| (D-Trp)$_{slow}$ | 0.15±0.01 | 0.01 | 1.07±0.13 | 0.23±0.01 | 0.02 | 0.62±0.18 | 0.65±0.04 |
| (L-Trp)$_{slow}$ | 0.14±0.01 | 0.01 | | 0.37±0.07 | 0.03 | | 0.37±0.09 |
| D-Ala | 7.69±0.25 | 0.69 | 1.52±0.29 | 7.06±0.08 | 0.63 | 1.20±0.11 | 1.09±0.26 |
| L-Ala | 6.87±0.15 | 0.45 | | 5.89±0.08 | 0.53 | | 0.86±0.17 |
| D-Ser | 4.59±0.06 | 0.41 | 0.67±0.02 | 3.70±0.06 | 0.34 | 0.49±0.01 | 1.24±0.05 |
| L-Ser | 5.05±0.05 | 0.62 | | 7.56±0.06 | 0.68 | | 0.91±0.02 |
| D-Thr | 2.89±0.04 | 0.25 | 0.81±0.03 | 2.79±0.05 | 0.24 | 0.78±0.05 | 1.03±0.04 |
| L-Thr | 3.56±0.08 | 0.30 | | 3.65±0.13 | 0.31 | | 0.97±0.06 |
| D-Athr | 1.75±0.07 | 0.15 | 0.40±0.03 | 2.49±0.01 | 0.21 | 0.57±0.01 | 0.70±0.03 |
| L-Athr | 4.35±0.09 | 0.37 | | 4.38±0.08 | 0.37 | | 0.99±0.04 |

**Kinetics and enantioselectivity of $[\mathbf{1}_L HA]^+$ (A=Tyr, TyrOMe) complexes**: As pointed out in a previous paper,[32] a quantitative estimate of the $[\mathbf{1}_L HA]^+$ energetics by MM calculations and MD simulations is prevented because of the high flexibility of the $\mathbf{1}_L$ host which makes the number of its conceivable adducts with the selected amino acids exceedingly large. Besides, any computational attempt to reproduce quantitatively the small activation free energy differences derived from the measured enantioselectivity values ($<2.5$ kJ mol$^{-1}$ at 300 K; Table 2) is thwarted by the relatively large uncertainty associated with the computational approaches. As a consequence, we can just provide a *qualitative* description of the structural features of the $[\mathbf{1}_L HA]^+$ adducts which, however, may reveal very helpful in rationalizing the FT-ICR experimental results. This is the case of the diastereomeric $[\mathbf{1}_L HTyr]^+$ and $[\mathbf{1}_L HTyrOMe]^+$ complexes, the first ones exhibiting mono-exponential kinetics with $\rho$ and $\xi$ below unit and the latter ones characterized by bi-exponential kinetics with $\rho<1$ and $\xi>1$.

As reported in the Computational Details section, a complete and reasonably homogeneous sampling of the whole potential energy hypersurface of the selected $[\mathbf{1}_L \cdot H \cdot A]^+$ systems requires the combination of docking studies with MD simulations. The time evolution of the molecular motions of the host and guest moieties, in fact, is expected to let the system move among many conformations populated at room temperature, by crossing over low energy barriers and by favouring large flat minima with respect to narrow ones, so as to provide a dynamic picture of the recognition process. Furthermore, energy minimizations in molecular mechanics (docking) give steric energies corresponding to enthalpies at 0 K. Therefore, to get average enthalpies at room temperature, more appropriate for large and flexible systems, a constant temperature MD simulation is needed.

Previous experimental and MCMM simulations revealed that the energetically most favoured $[\mathbf{1}_L HA]^+$ structures are invariably obtained by locating the proton between the amido groups signalled in Figure 1 by the broken circles. Indeed, location of the proton on one of the other amido groups is calculated to cost over 17 kJ mol$^{-1}$ more at 300 K.[32]

The results of docking calculations for the homochiral $[\mathbf{1}_L HTyr_L]^+$ and $[\mathbf{1}_L HTyrOMe_L]^+$ complexes are illustrated in Figure 4a and b, respectively. Similar patterns have been obtained with the corresponding heterochiral adducts. The distribution of the SD values shown in Figure 4a indicates that, at 0 K, $Tyr_L$

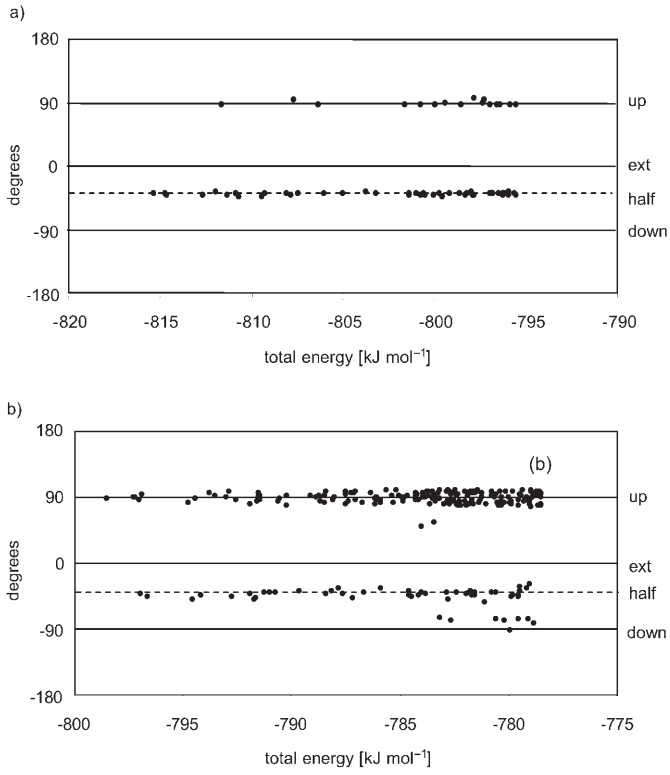


Figure 4. Docking of a) $[\mathbf{1}_L HTyr_L]^+$ and b) $[\mathbf{1}_L HTyrOMe_L]^+$.

  

preferentially occupies two specific regions of $[\mathbf{1}_L H]^+$. In fact, the lowest-energy MCMM/MOLS host–guest complexes, collected within 20 kJ mol$^{-1}$, exhibit a clear preference of $Tyr_L$ for regions of three-dimensional space at SD values ranging around +90° (the *up* region) or −40°. This latter value corresponds to a structure with the $Tyr_L$ guest placed halfway from both the *down* (SD = −90°) and *ext* (SD = 0°) regions of $[\mathbf{1}_L H]^+$ complex. This position is henceforth denoted as the *half* region. The distribution of the SD values shown in Figure 4b suggests that both the *up* and the *half* regions of $[\mathbf{1}_L H]^+$ are mostly suited for hosting $TyrOMe_L$ as well. In the latter case, $TyrOMe_L$ appears to be located at the most frequent SD value of about −45°, instead of the −40° value derived for the $Tyr_L$ guest (Figure 4b). This small difference indicates that, relative to $Tyr_L$, the $TyrOMe_L$ guest is located slightly more inwards the host cavity and more surrounded by its chiral pendants (Figure S13a and b, Supporting Information).

Molecular dynamics simulations on $[\mathbf{1}_L HTyr_L]^+$ suggest that, at 300 K, the amino acid guests can be permanently trapped nearby the chiral lower rim of $[\mathbf{1}_L H]^+$ (the *half* region; Figure 5b) as well as on its apparently achiral upper rim (the *up* region; Figure 5a). Similar patterns have been observed with the *up* and *half* structures of the diastereomeric $[\mathbf{1}_L HTyrOMe]^+$ complexes as well (Figure S14 of Supporting Information). The *half* and *up* regioisomers of either $[\mathbf{1}_L HTyrOMe_L]^+$ and $[\mathbf{1}_L HTyrOMe_D]^+$ exhibit almost the same average potential energy (within 1 kJ mol$^{-1}$), when scaled to 300 K. In contrast, the average potential energy of the *up* regioisomer of $[\mathbf{1}_L HTyr_L]^+$ exceeds that of the *half* regioisomer by 9 kJ mol$^{-1}$, in agreement with the largely predominant occurrence of the latter structure under the ESI-FT-ICR conditions.

The results of docking calculations and MD simulations on the *half* regioisomers of $[\mathbf{1}_L HTyr_L]^+$ (Figure 5b) and $[\mathbf{1}_L HTyrOMe]^+$ can be compared to those carried out in previous studies on the diastereomeric $[\mathbf{1}_L HDOPA]^+$ complexes.[32] In this case, several recognition geometries were found, characterized by SD values between −90 and 0°. Moreover, it was observed that, during MD simulations starting from *ext* geometries (SD ≈ 0°), DOPA moved towards the lower rim of $[\mathbf{1}_L{\cdot}H]^+$ (the *down* region). By this movement, the two phenolic OH of DOPA could form hydrogen bonds with the polar amido groups of the host at the lower rim. This final structure somewhat resembles the global minimum geometry of the complex $[\mathbf{1}_L HTyr_L]^+$ and $[1_L HTyrOMe_L]^+$ complexes, shown in Figure S13 of the Supporting Information. Differently from the case of DOPA, however, the "canyon-shaped" architecture adopted by the host appears to be less sharp when interacting with $Tyr_L$ and the TyrOMe enantiomers, probably due to the lack of the *meta* OH group in these guests which may allow the location of the guest slightly outside the host chiral cavity (SD($Tyr_L$) = −40 and SD(TyrOMe) = −45° vs SD(DOPA) = −90°) and, therefore, the establishment of more interactions among the host pendants.

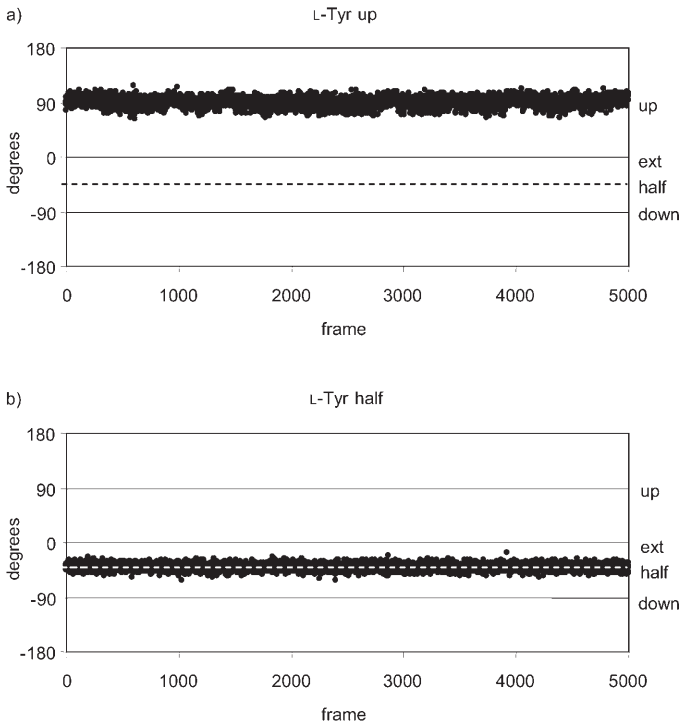


Figure 5. Molecular dynamics of a) *half* and b) *up* regioisomers of $[\mathbf{1}_L HTyr_L]^+$.

MD simulations have been also applied to the rotatable $C_{ring}$–$C_\alpha$ bond of the high-energy *up* $[\mathbf{1}_L HTyr_L]^+$ complex; its structural descriptor (SD) is illustrated in Figure 2b. The results of the MD runs are reported in Figure 6a together with the *up* geometry of the $[\mathbf{1}_L HDOPA_L]^+$ complex, shown in the inset. The SD values point to the fast interconversion of two guest geometries at the upper rim region of the host.

Analysis of Figure 6a helps clarifying the reasons why *up* $Tyr_L$ complexes are less stable than to the corresponding *half* structures. The main reason can be found in the fact that the aromatic ring of $Tyr_L$ lacks of the *meta*-OH group, which is present in DOPA. This causes a sort of "head-down" orientation adopted by $Tyr_L$ to integrate the π–π aromatic stacking at the upper rim of the host, with a fruitful $C_{arom}OH$···OMe interaction (atoms belonging to the guest are henceforth denoted in italic). As a consequence, the polar interactions between the amino acid group of the guest and the upper rim of the host are severely weakened.

Differently from $Tyr_L$, the *up* region of $[\mathbf{1}_L H]^+$ is almost as suited as the *half* one for hosting the TyrOMe enantiomers. Indeed, as pointed out above, at 300 K, both *up* $[\mathbf{1}_L HTyrOMe]^+$ complexes have an average enthalpy very close to that of the corresponding *half* complexes (within 1 kJ mol$^{-1}$). The results of MD simulations, applied to the rotatable $C_{ring}$–$C_\alpha$ bond of the *up* $[\mathbf{1}_L HTyrOMe_L]^+$ complex, are reported in Figure 6b. MD simulations on the *up* $[\mathbf{1}_L HTyrOMe_D]^+$ complex lead to the same picture. As for $[\mathbf{1}_L HTyr_L]^+$ (Figure 6a), the *up* structures of $[\mathbf{1}_L HTyrOMe]^+$ are characterized by the π–π aromatic stacking accompanied by *HN-H*···OMe and $C_{arom}OH$···OMe interactions. The evi-

  

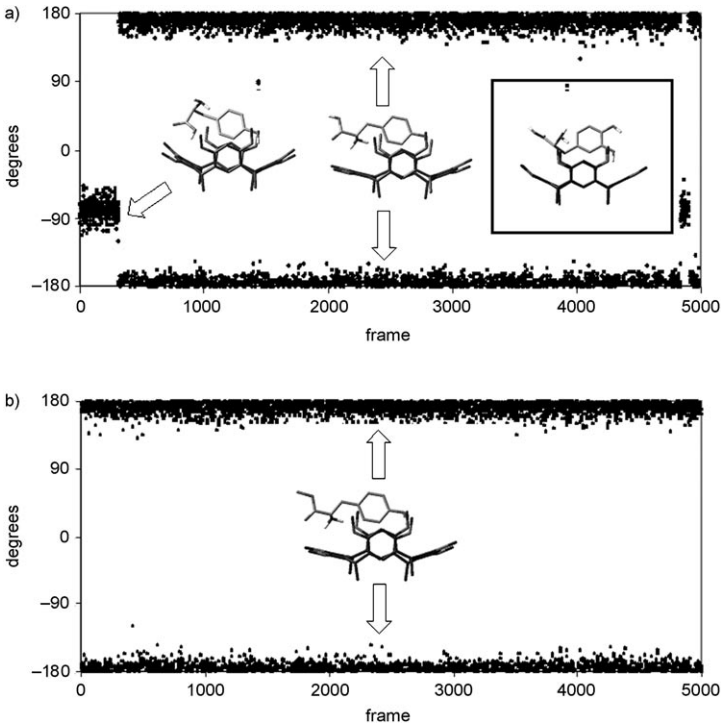


Figure 6. Molecular dynamics of the rotatable $C_{ring}$–$C_{\alpha}$ bond of the *up* regioisomers of a) $[\mathbf{1}_L HTyr_L]^+$ and b) $[\mathbf{1}_L HTyrOMe_L]^+$.

dent difference in the dynamics of $[\mathbf{1}_L HTyrOMe]^+$, by one side, and of $[\mathbf{1}_L HTyr_L]^+$, by the other, is to be attributed to the fact that, despite the co-operation of *HN-H*···OMe and $C_{arom}OH$···OMe interactions in all these structures, the $[\mathbf{1}_L HTyrOMe]^+$ complexes lack of a free acid group which allows the establishment of a *COOH*···OMe interaction to the expenses of the $C_{arom}OH$···OMe one. Besides, the stability of the *up* $[\mathbf{1}_L HTyrOMe_L]^+$ complex is enhanced by the presence of the freely rotating estereal group in TyrOMe which may establish additional dispersive interactions with the closest aromatic ring of the host.

The concomitant occurrence of stable *half* and *up* regioisomers of the $[\mathbf{1}_L HTyrOMe]^+$ complexes is consistent with their bi-exponential reaction kinetics (see Supporting Information). In analogy with the $[\mathbf{1}_L HDOPA]^+$ systems[32] and in qualitative agreement with the computed enthalpy gap between the *up* and *half* $[\mathbf{1}_L HTyrOMe]^+$ structures, the most stable *half* regioisomer is identified as the less reactive $([\mathbf{1}_L HTyrOMe]^+)_{slow}$ component and amounts to about 80% of the total ion abundance. The less stable *up* regioisomer is obviously identified as the most reactive $([\mathbf{1}_L HTyrOMe]^+)_{fast}$ component and accounts for the residual ca. 20% of the total ion abundance (Table 1). In contrast, the large stability gap between the *half* and *up* regioisomers of the $[\mathbf{1}_L HTyr]^+$ complexes (9 kJ mol$^{-1}$) prevents the formation of the latter one and, therefore, only the stable *half* regioisomer is formed under ESI-FT-ICR conditions. This accounts for the mono-exponential kinetics followed by the $[\mathbf{1}_L HTyr]^+$ complexes (see Supporting Information and Table 2).

The comparable $\rho < 1$ values, measured for the reaction with $[\mathbf{1}_L HTyr]^+$ and $[\mathbf{1}_L HTyrOMe]^+$, can be explained by the remarkable similarity of the corresponding *half* structures, both characterized by intense *C*=*O*···H–N and $C_{arom}OH$···O=C intermolecular interactions (Figure S13a,b of Supporting Information). The significant difference in the measured $\xi$ terms (Table 2) is due to the fact that, as pointed out before, TyrOMe is located more inwards the host cavity and surrounded by its chiral pendants than Tyr. As a consequence, relative to Tyr, displacement of TyrOMe requires that amine B enters more in depth into the host cavity which, therefore, may exert more the effects of its asymmetry towards it.

**Kinetics and enantioselectivity of $[\mathbf{1}_L HA]^+$ (A=Trp) complexes**: The computational protocol used for the $[\mathbf{1}_L HA]^+$ (A = Tyr, TyrOMe) systems has been extended to $[\mathbf{1}_L HTrp]^+$ as well. The results of docking calculations on the homochiral $[\mathbf{1}_L HTrp_L]^+$ and the heterochiral $[\mathbf{1}_L HTrp_D]^+$complexes are shown in Figure 7a and b, respectively. The distribution of the relevant SD values as a function of the energy of output complexes (<20 kJ mol$^{-1}$ over the global minimum) points to both Trp enantiomers as residing preferentially at the *up* and *down* regions of the $[\mathbf{1}_L H]^+$ host.

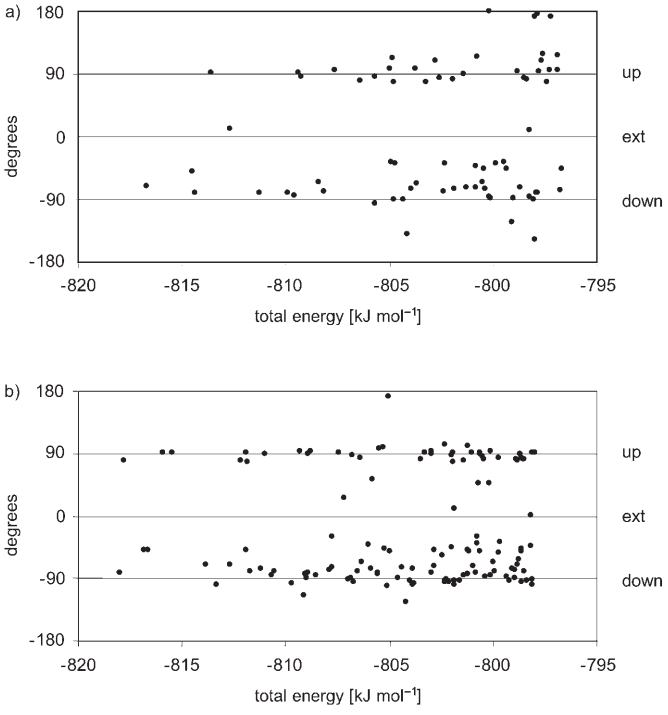


Figure 7. Docking of a) $[\mathbf{1}_L HTrp_L]^+$ and b) $[\mathbf{1}_L HTrp_D]^+$.

Molecular dynamics simulations starting from the global minima of $[\mathbf{1}_L HTrp_D]^+$ suggest that the guest can be permanently trapped in the chiral lower rim of the $[\mathbf{1}_L H]^+$ (the *down* region) as well as in its apparently achiral upper rim (the *up* region) (Figure S15 of Supporting Information).

  

Similar patterns have been observed with $[\mathbf{1}_L HTrp_L]^+$ as well (Figure S16 of Supporting Information). The occurrence of stable *down* and *up* structures for the diastereomeric $[\mathbf{1}_L HTrp]^+$ complexes accounts for their bi-exponential reaction kinetics ((Figure S3 and S4 of Supporting Information). The average potential energy gaps, scaled to 300 K, between the *down* and *up* regioisomers of $[\mathbf{1}_L HTrp_D]^+$ and $[\mathbf{1}_L HTrp_L]^+$ amount to 3 and 8 kJ mol$^{-1}$, respectively, in favour of the *down* structures. The more stable *down* structures are associated with the most abundant $([\mathbf{1}_L HTrp]^+)_{slow}$ fractions (65–68%; Table 1), while the less stable *up* one with the less abundant $([\mathbf{1}_L HTrp]^+)_{fast}$ components (32–35%; Table 1).

The average enthalpies of complexation of the diastereomeric $[\mathbf{1}_L HTrp]^+$ structures $[\Delta\Delta H_{av} = (\Delta H_{av})_{homo} - (\Delta H_{av})_{hetero}]$, calculated from the difference between the average combined enthalpy of the two isolated components and that of the complexes, are estimated to amount to $-7$ and $-2$ kJ mol$^{-1}$ for the *down* and *up* structures, respectively.[50] Let us now consider these stability gaps in the light of the structures of the relevant global minima (Figure 8).

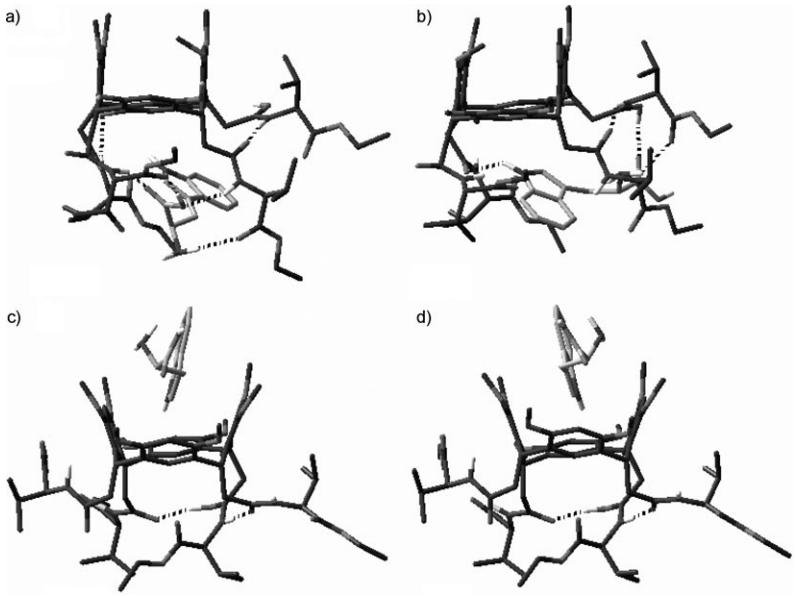


Figure 8. Front view of the fully minimized structures of: 1) the *down* regioisomers of a) $[\mathbf{1}_L{\cdot}H{\cdot}Trp_D]^+$ and b) $[\mathbf{1}_L{\cdot}H{\cdot}Trp_L]^+$ complexes; 2) the *up* regioisomers of c) $[\mathbf{1}_L{\cdot}H{\cdot}Trp_L]^+$ and d) $[\mathbf{1}_L{\cdot}H{\cdot}Trp_D]^+$ complexes. Hydrogen-bonding interactions are depicted as dotted lines.

The distribution of SD values shown in Figure 7 suggests that, in contrast to DOPA, the *ext* region of $[\mathbf{1}_L H]^+$ is not suitable for hosting Trp. This different behavior is probably caused by the absence of appropriate OH "hooks" on the Trp aromatic rings. Indeed, their presence in DOPA allows the formation of high-energy *ext* structures. The observation that, like Trp, both Tyr and TyrOMe never reside at the *ext* region of $[\mathbf{1}_L H]^+$ suggests that the presence of only one OH "hook" on their aromatic ring is not enough for the formation of the *ext* structure.

In spite of the evident differences in the complexation modes, chiral recognition of DOPA and Trp by $[\mathbf{1}_L H]^+$ exhibits close similarities. The steric energy difference between the relevant *up* and *down* structures is indeed rather close and unaffected by the configuration of the amino acid guest (the global minima of the diastereomeric complexes are quasi-degenerate). In analogy with DOPA, the $[\mathbf{1}_L H]^+$ host adopts a pre-organized "canyon-shaped" architecture by hydrogen bondings between adjacent pendants to embody Trp. Such hydrogen bonds are maintained during the MD runs and, therefore, the indole moiety of Trp is firmly accommodated in the "canyon-shaped" cleft, where it finds sterically complementary and electronically appropriate surfaces of the host. However, according to Figure 8a, the amino acid groups of $Trp_D$ interact with two different chiral pendants of the host (four hydrogen bonds), while in the case of $Trp_L$, the indolic NH and the amino acid groups form three hydrogen bonds with two different host pendants (Figure 8b). These different interactions are responsible of the quasi-orthogonal orientation of the Trp enantiomers in the *down* cavity of $[\mathbf{1}_L H]^+$. The consequence is a different host/guest packing for the relevant *down* $[\mathbf{1}_L HTrp]^+$ structures which may account for the opposite $\rho$($>1$ with $B_R$; $<1$ with $B_S$) and the largely different $\xi$ enantioselectivity factors, measured for $([\mathbf{1}_L HTrp]^+)_{slow}$ (Table 2).

The reasons of the *up*-trapping of Trp can be certainly ascribed to both the low polarity of the guest and the structure of its side chain, which allow the guest to establish a very effective π–π stacking interaction with the electron-rich cavity at the upper rim of the host, strengthened by a dipolar interaction of the NH group, properly located between the methoxy groups of two facing aromatic rings (Figure 8c, d). Such a favourable spatial orientation shows close analogies with that of the complex with DOPA, wherein the dipolar interaction of the indole NH functionality is replaced by that of the *meta*-OH group (inset of Figure 6a). In this connection, the similar $\rho$ and $\xi$ values, measured for the *up* and *down* $[\mathbf{1}_L HTrp]^+$ structures, are rather surprising since, differently from *down* regioisomers, the *up* ones display a lower-rim cavity which is not appreciably perturbed by the presence of the guest (Figure 8c,d). Thus, no appreciable enantioselectivity ($\rho \approx 1$) would be expected in the reaction of the $[\mathbf{1}_L HTrp]^+$ *up* regioisomers with both amine enantiomers. In contrast, $\rho = 1.60 \pm 0.11$ (with $B_R$) and $\rho = 0.82 \pm 0.10$ (with $B_S$) (Table 2). However, a closer inspec-

  

tion of Figure 8c,d reveals that the $[\mathbf{1}_L\text{HTrp}]^+$ *up* structures do have a molecular chirality due to the bent position of the guest in the upper-rim cavity of the host. Therefore, despite the chiral lower-rim cavity of the diastereomeric $[\mathbf{1}_L\text{HTrp}]^+$ *up* complexes is unaffected by the guest, nevertheless its presence at the *up* region of the host generates two supramolecular diastereomeric forms which may be responsible of the observed enantioselectivity. In other words, the enantioselective behaviour of the diastereomeric $[\mathbf{1}_L\text{HTrp}]^+$ *up* complexes towards the amine enantiomers leads one to conjecture on the occurrence of a heterotropic allosteric effect in these supramolecular systems.[51]

**Kinetics and enantioselectivity of $[\mathbf{1}_L\text{HA}]^+$ (A=Thr, AThr) complexes**: As shown in Table 2, the $[\mathbf{1}_L\text{HA}]^+$ (A=Thr, AThr) systems follow mono-exponential kinetics much like the $[\mathbf{1}_L\text{HSer}]^+$ one. As pointed out in previous papers,[31,32] this kinetic behaviour is due to: i) the exclusive formation of a single stable regioisomer, for example, the *down* structure for $[\mathbf{1}_L\text{HSer}_D]^+$; or ii) several unstable regioisomers with the guest moving fast around the host on the reaction time scale, for example, all $[\mathbf{1}_L\text{HSer}_L]^+$ regioisomers rapidly moving over both the *ext* and the *down* regions of the host. Enantioselectivity of $[\mathbf{1}_L\text{HSer}]^+$ is mainly controlled by the relative stability of the diastereomeric complexes ($\rho<1$) and by the specific path followed by B for removing serine ($\xi>1$ with the *down* $[\mathbf{1}_L\text{HSer}_D]^+$ structure and $\xi\leq1$ with the rapidly interconverting $[\mathbf{1}_L\text{HSer}_L]^+$ ones). The reaction efficiencies and the enantioselectivity parameters, measured with the $[\mathbf{1}_L\text{HA}]^+$ (A=Thr, AThr) systems, are qualitatively similar to those obtained with $[\mathbf{1}_L\text{HSer}]^+$, thus suggesting a distinct prevalence of the stable *down* regioisomer for the heterochiral complexes and of rapidly interconverting structures for the homochiral ones.

Comparative analysis of the kinetic results for $[\mathbf{1}_L\text{HA}]^+$ (A=Ser, Thr, AThr) points to an appreciable decrease of the reaction efficiency in going from $[\mathbf{1}_L\text{HSer}_D]^+$ to $[\mathbf{1}_L\text{HThr}_D]^+$ to $[\mathbf{1}_L\text{HAThr}_D]^+$ (Table 2), while their homochiral analogues follow a different efficiency order, that is, $[\mathbf{1}_L\text{HSer}_L]^+ > [\mathbf{1}_L\text{HAThr}_L]^+ > [\mathbf{1}_L\text{HThr}_L]^+$. These different trends have to be ascribed to the presence and the configuration of the chiral C(3) center of the amino acid and its effects on the relevant adduct structures. The limited effect of the B configuration on the reaction efficiencies of the homochiral $[\mathbf{1}_L\text{HA}_L]^+$ (A=$\text{Ser}_L$, $\text{Thr}_L$, $\text{AThr}_L$) complexes ($0.91\leq\xi\leq0.99$; Table 2) confirms that the guest may move around all the host positions, including the *ext* one. In this case, amine B can remove the amino acid guest without entering the chiral-lower rim cavity of the host. The $[\mathbf{1}_L\text{HSer}_L]^+ > [\mathbf{1}_L\text{HAThr}_L]^+ > [\mathbf{1}_L\text{HThr}_L]^+$ efficiency trend probably reflects a reverse $[\mathbf{1}_L\text{HA}]^+$ stability order. On the contrary, the largely variable effect of the B configuration on the reaction efficiency of the heterochiral $[\mathbf{1}_L\text{HA}_D]^+$ (A=$\text{Ser}_D$, $\text{Thr}_D$, $\text{AThr}_D$) complexes ($0.70\leq\xi\leq1.24$; Table 1) complies with a stable *down* structure for these complexes. Here, amine B must partially enter the host chiral cavity to oust the amino acid guest through the involvement of a more congested, high-energy transition structure. The relatively small efficiencies, measured for the heterochiral complexes, further support this view. In this frame, the $[\mathbf{1}_L\text{HSer}_D]^+ > [\mathbf{1}_L\text{HThr}_D]^+ > [\mathbf{1}_L\text{HAThr}_D]^+$ efficiency trend (Table 2) may be regarded as due to increasingly congested transition structures in the *down* region of the $[\mathbf{1}_L\text{H}]^+$ host.

## Conclusion

The gas-phase base-induced displacement reaction between the 2-aminobutane enantiomers (B) and the diastereomeric $[\mathbf{1}_L\text{HA}]^+$ complexes (A=amino acid) exhibits a significant enantioselectivity which has been discussed in the light of molecular mechanics calculations and molecular dynamics simulations. A comprehensive analysis of the experimental and computational results extends and reinforces previous conclusions that the enantioselectivity of these reaction are mainly determined by the effects of the host asymmetric frame upon the structure and the stability of the diastereomeric $[\mathbf{1}_L\text{HA}]^+$ complexes and the orientation of the amine reactant B in its encounters with them.

In particular, the $[\mathbf{1}_L\text{HA}]^+$ complexes can be classified in three broad categories: i) those in which the amino acid guest does not present any additional functionality besides the amino acid one (Ala, Phg, and Phe); ii) those in which the amino acid guest presents an additional alcoholic function (Ser, Thr, and AThr); and iii) those in which the amino acid guest contains several additional functionalities on its aromatic ring (Tyr, TyrOMe, Trp, and DOPA). Reaction (1) with class i) complexes is characterized by an appreciable sensitivity to the configuration of A ($\rho>1$), but it is essentially unaffected by that of B ($\xi\approx1$). Reaction (1) with class ii) complexes exhibits an appreciable sensitivity to both the A and B configuration ($\rho<1$; $\xi\neq1$). Reaction (1) with class iii) complexes displays a significant sensitivity both to the A and B configuration which markedly depends on the functionalities of guest A. The origin of these pronounced selectivity differences may be mainly attributed to the effects of the $\mathbf{1}_L$ asymmetric frame upon the structure and the stability of the diastereomeric transition structures involved in Reaction (1). Thus, class i) enantioselectivities are attributed to the attack of the amine B on the amino acid guest placed outside the host in proximity of two adjacent pendants (the *ext* region). Class ii) enantioselectivities are determined by the greater stability of the heterochiral $[\mathbf{1}_L\text{HA}_D]^+$ *down* complexes, relative to that of their homochiral $[\mathbf{1}_L\text{HA}_L]^+$ *ext* analogues. In class iii complexes, the amino acid guest may permanently occupy both the *up* and *down* (or *half*) regions of the host (A=TyrOMe, Trp, and DOPA) or just the last one (A=Tyr). Their occurrence accounts for the observation of bi-exponential reaction kinetics in the first case and of mono-exponential ones in the latter. The large variations in class iii) enantioselectivities are attributed to the specific effects of the A functionalities on its location in the *up* and *down* (or *half*) regions of the host. The results of this comprehensive investigation may be regarded as contributing to

  

the formulation of a model for chiral recognition of biomolecules by enzyme mimics in the unsolvated state.

## Acknowledgement

Work supported by the Ministero dell'Istruzione dell'Università e della Ricerca (MIUR, COFIN), the Consiglio Nazionale delle Ricerche (CNR) and Istituto Pasteur Fondazione Cenci Bolognetti. B.B. and A.T. gratefully acknowledge Project "FIRB 2003" from MIUR (Ministero della Università e della Ricerca). The authors express their gratitude to F. Angelelli for technical assistance.

[1] M. Sawada, *Biological Mass Spectrometry: Present and Future* (Eds.: T. Matsuo, R. M. Caprioli, M. L. Gross, T. Seyama), Wiley, New York, **1994**, p. 639–646.
[2] M. Sawada, *Mass Spectrom. Rev.* **1997**, *16*, 73–90.
[3] C. A. Schalley, *Int. J. Mass Spectrom.* **2000**, *194*, 11–39.
[4] A. Filippi, A. Giardini, S. Piccirillo, M. Speranza, *Int. J. Mass Spectrom.* **2000**, *198*, 137–163.
[5] C. B. Lebrilla, *Acc. Chem. Res.* **2001**, *34*, 653–661.
[6] D. V. Dearden, Y. Liang, J. B. Nicoll, K. A. Kellersberger, *J. Mass Spectrom.* **2001**, *36*, 989–997.
[7] C. A. Schalley, *Mass Spectrom. Rev.* **2001**, *20*, 254–309.
[8] M. Speranza, *Adv. Phys. Org. Chem.* **2004**, *39*, 147–281.
[9] M. Speranza, *Int. J. Mass Spectrom.* **2004**, *232*, 277–317.
[10] M. Speranza, M. Satta, S. Piccirillo, F. Rondino, A. Paladini, A. Giardini, A. Filippi, D. Catone, *Mass Spectrom. Rev.* **2005**, *24*, 588–610.
[11] K. A. Schug, W. Lindner, *J. Sep. Sci.* **2005**, *288*, 1932–1955.
[12] M. G. Finn, *Chirality* **2002**, *14*, 534–540.
[13] J. S. Splitter, F. Turecek, *Applications of Mass Spectrometry to Organic Stereoselectivity*, VCH, New York, **1994**.
[14] E. N. Nikolaev, E. V. Denisov, V. S. Rakov, J. H. Futrell, *Int. J. Mass Spectrom.* **1999**, *183*, 357–368.
[15] D. V. Dearden, Y. Liang, J. B. Nicoll, K. A. Kellersberger, *J. Mass Spectrom.* **2001**, *36*, 989–997.
[16] Y. Liang, J. S. Bradshaw, D. V. Dearden, *J. Phys. Chem. A* **2002**, *106*, 9665–9671.
[17] K. Vékey, G. Czira, *Rapid Commun. Mass Spectrom.* **1995**, *9*, 783–787.
[18] W. A. Tao, L. Wu, R. G. Cooks, *Chem. Commun.* **2000**, 2023–2024.
[19] W. A. Tao, R. G. Cooks, *Anal. Chem.* **2003**, *75*, 25A–31A.
[20] W. A. Tao, D. Zhang, E. N. Nikolaev, R. G. Cooks, *J. Am. Chem. Soc.* **2000**, *122*, 10598–10609.
[21] W. A. Tao, R. G. Cooks, *Eur. J. Mass Spectrom.* **2002**, *8*, 107–115.
[22] W. A. Tao, R. L. Clark, R. G. Cooks, *Anal. Chem.* **2002**, *74*, 3783–3789.
[23] W. A. Tao, R. G. Cooks, *Angew. Chem.* **2001**, *113*, 779–782; *Angew. Chem. Int. Ed.* **2001**, *40*, 757–760.
[24] W. A. Tao, F. G. Gozzo, R. G. Cooks, *Anal. Chem.* **2001**, *73*, 1692–1698.
[25] L. Wu, R. G. Cooks, *Anal. Chem.* **2003**, *75*, 678–684.
[26] J. Ramirez, F. He, C. B. Lebrilla, *J. Am. Chem. Soc.* **1998**, *120*, 7387–7388.
[27] J. Ramirez, S. Ahn, G. Grigorean, C. B. Lebrilla, *J. Am. Chem. Soc.* **2000**, *122*, 6884–6890.
[28] J. F. Gal, M. Stone, C. B. Lebrilla, *Int. J. Mass Spectrom.* **2003**, *222*, 259–267.
[29] S. Ahn, J. Ramirez, G. Grigorean, C. B. Lebrilla, *J. Am. Soc. Mass Spectrom.* **2001**, *12*, 278–287.
[30] G. Grigorean, C. B. Lebrilla, *Anal. Chem.* **2001**, *73*, 1684–1691.
[31] B. Botta, M. Botta, A. Filippi, A. Tafi, G. Delle Monache, M. Speranza, *J. Am. Chem. Soc.* **2002**, *124*, 7658–7659.
[32] A. Tafi, B. Botta, M. Botta, G. Delle Monache, A. Filippi, M. Speranza, *Chem. Eur. J.* **2004**, *10*, 4126–4135.
[33] B. Botta, D. Subissati, A. Tafi, G. Delle Monache, A. Filippi, M. Speranza, *Angew. Chem.* **2004**, *116*, 4871–4874; *Angew. Chem. Int. Ed.* **2004**, *43*, 4767–4770.
[34] A. Filippi, M. Speranza, *Int. J. Mass Spectrom.* **2000**, *199*, 211–219.
[35] H. Bagheri, H. Chen, R. G. Cooks, *Chem. Commun.* **2004**, 2740–2741.
[36] C. D. Gutsche, *Calixarenes: Monographs in Supramolecular Chemistry* (Ed.: J. F. Stoddart), Royal Society of Chemistry, Cambridge, **1989**.
[37] C. D. Gutsche, *Calixarenes Revisited: Monographs in Supramolecular Chemistry* (Ed.: J. F. Stoddart), Royal Society of Chemistry, Cambridge, **1998**.
[38] "Calixarenes: A Versatile Class of Macrocyclic Compounds": *Topics in Inclusion Science, Vol. III* (Eds.: J. Vicens, V. Böhmer), Kluwer Academic Publishers, Dordrecht, The Netherlands, **1991**.
[39] V. Böhmer, *Angew. Chem.* **1995**, *107*, 785–818; *Angew. Chem. Int. Ed. Engl.* **1995**, *34*, 713–745.
[40] A. M. A. van Wageningen, W. Verboom, D. N. Reinhoudt, *Pure Appl. Chem.* **1996**, *68*, 1273–1277.
[41] A. Ikeda, S. Shinkai, *Chem. Rev.* **1997**, *97*, 1713–1734.
[42] *Calixarenes in Action* (Eds.: L. Mandolini, R. Ungaro), Imperial College Press, London, **2000**.
[43] Z. Asfari, V. Böhmer, J. Harrowfield, J. Vicens, *Calixarenes 2001*, Kluwer Academic Publishers, Dordrecht, The Netherlands, **2001**.
[44] J. M. Harrowfield, W. R. Richmond, A. N. Sobolev, A. H. White, *J. Chem. Soc. Perkin Trans. 2* **1994**, 5–9.
[45] R. Ludwig, *Fresenius, J. Anal. Chem.* **2000**, *367*, 103–128.
[46] G. Arena, A. Contino, A. Magri, D. Sciotto, G. Spoto, A. Torrisi, *Ind. Eng. Chem. Res.* **2000**, *39*, 3605–3610.
[47] B. Botta, G. Delle Monache, P. Salvatore, F. Gasparrini, C. Villani, M. Botta, F. Corelli, A. Tafi, E. Gacs-Baitz, A. Santini, C. F. Carvalho, D. Misiti, *J. Org. Chem.* **1997**, *62*, 932–938.
[48] F. Mohamadi, N. G. J. Richards, W. C. Guida, R. Liskamp, M. Lipton, C. Caufield, G. Chang, T. Hendrickson, W. C. Still, *J. Comput. Chem.* **1990**, *11*, 440–467.
[49] T. Su, *J. Phys. Chem.* **1988**, *88*, 4102–4103; T. Su, *J. Phys. Chem.* **1988**, *88*, 5355.
[50] S. Chimin, K. N. Houk, *J. Am. Chem. Soc.* **1996**, *118*, 8056–8070.
[51] a) B. Botta, F. Caporuscio, D. Subissati, A. Tafi, M. Botta, A. Filippi, M. Speranza, *Angew. Chem.* **2006**, *118*, 2783–2786; *Angew. Chem. Int. Ed.* **2006**, *45*, 2717-2720.

Received: January 23, 2006
Revised: March 28, 2006
Published online: July 31, 2006

  